Doping dependence of chiral superconductivity in near 45° twisted bilayer cuprates

Mathieu Bélanger and David Sénéchal
Département de physique and Institut quantique, Université de Sherbrooke, Sherbrooke, Québec, Canada J1K 2R1

(Received 8 June 2023; revised 7 December 2023; accepted 18 December 2023; published 5 January 2024)

We study a one-band Hubbard model for a twisted cuprate bilayer with a twist angle of 43.6° and a moiré cell containing 58 sites. We use the variational cluster approximation (VCA), which treats short-range correlations exactly and leads, in single layers, to a dome of d-wave superconductivity away from half filling from strong on-site repulsion alone. We find a time-reversal-symmetry (TRS) breaking phase in a small doping interval in the overdoped region when interlayer tunneling is strong enough. Contrary to expectations, being closer to the 45° twist angle does not expand this TRS region compared to a previous study [Lu and Sénéchal, Phys. Rev. B **105**, 245127 (2022)] on a 53° twist angle. This is attributed to the fact that the two superconducting states in competition have almost identical nodal structures.

DOI: 10.1103/PhysRevB.109.045111

I. INTRODUCTION

The observation of unconventional superconductivity in twisted bilayer graphene [1,2] has motivated similar studies on various van der Waals heterostructures [3], like twisted boron nitride [4] and transition metal dichalcogenides [5–12]. Those systems offer more degrees of freedom than their monolayer counterparts due to the twist angle, which can be changed.

The realization of a two-dimensional monolayer of $Bi_2Sr_2CaCu_2O_{8+\delta}$ (Bi2212) [13,14] has motivated research on twistronics in cuprates [15–19]. It has been predicted that a fully gapped, time-reversal symmetry (TRS) breaking $d_{x^2-y^2} + id_{xy}$ superconducting phase will emerge in systems with twist angles close to 45° [15]. This superconducting phase is predicted to be topologically nontrivial. Chiral topological superconductivity is also predicted in twisted multilayer nodal superconductors [20].

The bilayer cuprate systems are natural Josephson junctions. Realizing those junctions in the laboratory is challenging due to disorder that may be introduced while preparing the sample [21,22]. An early study of a c-axis twisted cuprate Josephson junction did not show the expected d-wave behavior [23]. New processes have been proposed to create those junctions and offer evidence that the Josephson current is reduced close to 45° due to a mismatch between the d-wave states of the two layers [21,22,24]. The critical current might remain finite at 45°, pointing to a state with TRS breaking [25]. Such behavior was predicted using simple models describing twisted bilayer cuprates [26,27].

Previous theoretical work based on the Bogoliubov–de Gennes mean-field theory lacks the effect of strong correlation, which is important in cuprates. Moreover, the physics of cuprates is strongly doping dependent, being affected by the pseudogap phenomenon below optimal doping [28]. A twisted t-J model of cuprates within slave-boson mean-field theory predicts that the range of twist angle around 45° which allows TRS breaking is narrow [29]. To address the effect of the strong correlation and the effect of doping, a Hubbard model for a system with a twist angle of $\theta = 53.13°$ has been studied with the variational cluster approximation (VCA) and cluster dynamical mean-field theory [17]. TRS breaking was observed near optimal doping when strong interlayer tunneling was considered. It was conjectured that at a twist angle closer to 45°, the mixed state could be more stable as a function of doping. The number of orbitals per unit cell in systems close to 45° makes them challenging to study using quantum cluster methods.

In this paper we take a step further into studying systems close to 45° by considering a Hubbard model for bilayer cuprates at a twist angle $\theta = 43.60°$, corresponding to a unit cell of 58 copper sites. We use the VCA to probe the stability of the TRS-breaking superconducting phase against doping. We follow the methodology proposed in Ref. [17] and show that a TRS-breaking phase occurs again in a narrow doping range, which can be explained by the band structure limiting the energy gained from combining the two superconducting states in competition. Thus, moving closer to a 45° twist angle does not necessarily stabilize the TRS-breaking phase, which is counterintuitive.

II. MODEL AND METHOD

A. Model

We use the tight-binding Hubbard model proposed in Ref. [17], in which each layer is described by a one-band Hubbard model, each site corresponding to a copper atom. The Hamiltonian can be separated as

$$H = H^{(1)} + H^{(2)} + H_\perp, \tag{1}$$

where the intralayer Hamiltonian $H^{(l)}$ is

$$H^{(l)} = \sum_{\mathbf{r},\mathbf{r}'\in l,\sigma} t_{\mathbf{r}\mathbf{r}'} c^\dagger_{\mathbf{r},l,\sigma} c_{\mathbf{r}',l,\sigma} + U \sum_{\mathbf{r}} n_{\mathbf{r},l,\uparrow} n_{\mathbf{r},l,\downarrow} - \mu \sum_{\mathbf{r},\sigma} n_{\mathbf{r},l,\sigma}, \tag{2}$$

where $c_{\mathbf{r},l,\sigma}$ ($c^\dagger_{\mathbf{r},l,\sigma}$) is the annihilation (creation) operator of an electron at site $\mathbf{r}$ on layer l ($l = 1, 2$) with spin $\sigma = \uparrow, \downarrow$ and $n_{\mathbf{r},l,\sigma}$ is the number operator. $\mathbf{r}$ and $\mathbf{r}'$ are the site indices of a square lattice for each layer. U is the on-site repulsion between electrons, and $t_{\mathbf{r}\mathbf{r}'}$ is the hopping matrix that includes nearest-neighbor hopping t and next-nearest-neighbor hopping t'. No extended interaction terms were considered since strongly correlated superconductivity can be driven by local repulsion alone and has been shown to be resilient to extended Coulomb repulsion at intermediate to strong coupling [30]. In Bi2212, the nearest-neighbor hopping is $t = 126$ meV [31], but here we use t as the energy unit. To describe Bi2212 we use the set of parameters $t = 1, t' = -0.3$, and $U = 8$ [17,31]. We also test other parameter sets (Sec. III B) to assess the robustness of our results.

The effect of the twist angle comes from the interlayer tunneling given by

$$H_\perp = \sum_{n=1}^{7} V_n \sum_{\langle \mathbf{r},\mathbf{r}'\rangle_{\perp,n,\sigma}} [c^\dagger_{\mathbf{r},1,\sigma} c_{\mathbf{r}',2,\sigma} + \text{H.c.}], \tag{3}$$

with $\langle \mathbf{r}, \mathbf{r}'\rangle_{\perp,n,\sigma}$ representing the set of sites $\mathbf{r}$ on layer 1 and $\mathbf{r}'$ on layer 2 such that their projections on the plane are nth neighbors. We will explain below why we consider interlayer hopping up to seventh interlayer neighbors. The strength of the tunneling is given by

$$V_n = V e^{-\lambda(|\mathbf{d_n}|-d_z)/a}, \tag{4}$$

where $|\mathbf{d_n}| = |\mathbf{r} - \mathbf{r}'|$ is the three-dimensional distance between the two sites corresponding to the nth neighbors on different layers, d_z is the distance between the two layers, and a is the lattice constant of the square lattice. V is the interlayer tunneling of sites that are on top of each other. λ is a damping parameter. To have a set of parameters similar to the one used in Ref. [17], we chose $d_z = a$ and $\lambda = 11.13$ with two different values of V: 0.2 and 0.4.

This model is a simplification of the real situation in bilayer cuprates. The effect of the rare-earth layers intercalated between CuO_2 planes is doubtless more complex. The model also neglects the fact that each monolayer of Bi2212 contains two CuO_2 planes. The values of the interlayer tunneling parameters chosen here are very strong and should be lower in order to better describe real twisted bilayers. Indeed, local-density approximation calculations [31] for bulk Bi2212 point to an interlayer hopping $t_z/t \approx 0.1$, smaller than our $V = 0.2$ or 0.4. These strong values of V are needed to observe TRS breaking in our system [17]. For interlayer hopping between sites that are not directly superimposed, adopting the exponential model (4) is both practical and reasonable since it allows comparisons between different twist angles while keeping the hopping parameters fixed. Overall, the effective model used here allows us to roughly delimit the range of parameters needed for chiral superconductivity to exist and to conclude whether that phase is within or beyond the reach of experiments on Bi2212 bilayers.

In this work we consider a system with a twist angle $\theta = 43.60^\circ$ in order to probe TRS breaking close to the optimal twist angle. Only a few twist angles correspond to commensurate systems with a reasonably small unit cell allowing for a microscopic description based on the Hubbard model [15]. This drastically limits the twist angles that can be studied. In Ref. [17], a 10-site unit cell with a twist angle of $\theta = 53.13^\circ$ was used. The next simplest case is the one studied here, a 58-site unit cell with a twist angle of $\theta = 43.60^\circ$. The next simpler case would correspond to a twist angle of $\theta = 45.24^\circ$ with 338 sites in the unit cell, quite beyond our computing capacity. Our goal is not to investigate all possible twist angles, but to see whether inching closer to a 45° twist changes the doping range over which a TRS-breaking superconducting state can be found.

B. Method

To probe the superconducting state in this model, we use the VCA [32,33] with an exact diagonalization solver at zero temperature. This is a variational approach on the electron self-energy which allows broken symmetries while treating short-range dynamical correlations exactly. It has been applied to magnetic phases [33–35] and superconductivity [12,36,37] in various systems. For a detailed review of the method, see Refs. [38,39]. The VCA is based on a cluster decomposition of the system: the infinite lattice is tiled with identical clusters small enough for the model to be solved exactly on each of them. Each cluster's Hamiltonian is basically a restriction of the lattice Hamiltonian to the cluster, plus one or more *Weiss fields*, whose role is to approximately represent the effect of the cluster's environment (the rest of the lattice) on the cluster's self-energy. The VCA proceeds by optimizing the Potthoff self-energy functional as a function of these Weiss fields. The optimal self-energy is subsequently applied to the whole lattice, and this provides an expression for the Green's function of the lattice problem, which can be used to compute the average of any one-body or anomalous operator. We use a restricted Nambu formalism to describe superconductivity, in which a particle-hole transformation was applied to the spin-down operators $c^\dagger_{\mathbf{r},l,\downarrow}$, allowing hopping terms and pairing terms to be treated on the same footing.

The use of exact diagonalization limits the total number of orbitals in a cluster to about 12 because of the computational resources needed to compute the Green's function. Considering this, we need to separate the 58-site unit cell in clusters of smaller sizes. We partitioned the unit cell into six clusters, as shown in Fig. 1: one cluster of 2 sites (labeled C), one cluster of 8 sites (labeled B), and four clusters of 12 sites each (labeled A). The basic approximation of cluster methods is to neglect the components $\Sigma_{ij}(\omega)$ of the self-energy matrix for which sites i and j belong to different clusters. The self-energy matrix $\mathbf{\Sigma}(\omega)$ is thus block diagonal, with each block being associated with a cluster. In the partition chosen here, blocks associated with clusters A, B, and C are of size 24, 16, and 4, respectively (there is a factor of 2 compared to cluster size because of the spin/Nambu degree of freedom).

The specific partition illustrated in Fig. 1 is not the only one possible, but it is one in which every cluster but C contains full 2×2 plaquettes in each layer. A successful description of strongly correlated superconductivity in the single-layer Hubbard model with cluster methods minimally requires a 2×2 plaquette [36,40]. Other partitions without this property

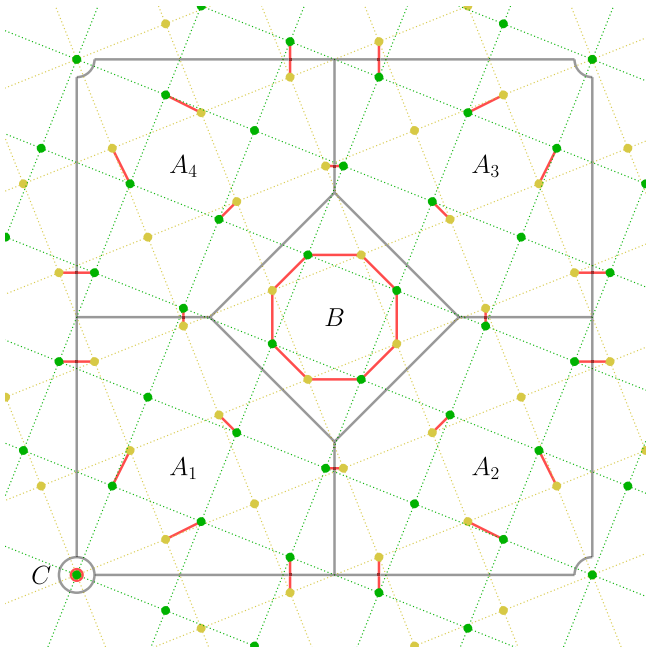

FIG. 1. Unit cell of the twisted cuprate system at $\theta = 43.60°$. It contains 58 sites between the two layers (green and yellow). The four A_i clusters contain 12 sites (6 from each layer), the B cluster contains 8 sites, and the C cluster contains only 2 sites that are on top of each other. The interlayer hopping amplitudes kept in our analysis are shown in red. The largest one (V) occurs between superimposed sites (cluster C). The interlayer amplitudes in cluster B are $0.24V$ (shorter bond) and $0.2V$ (longer bond), with our choice of λ [see Eq. (4)].

were tried but were problematic within the VCA, for instance, leading to discontinuities in the Potthoff functional, etc.

We keep interlayer hopping up to seventh interlayer neighbors in order to ensure that every cluster contains interlayer hopping. This also allows comparison with Ref. [17]. Note that the corresponding lateral physical distances are still smaller than the nearest-neighbor distance within each layer. For the sake of illustration, the exponential hopping model (4) leads to an interlayer hopping amplitude between adjacent sites of cluster B in the range $0.2V$ to $0.24V$.

C. Superconducting order parameter

The superconducting gap in single-layer or bulk cuprates has $d_{x^2-y^2}$ symmetry. This is well understood in theoretical studies of the doped, square-lattice Hubbard model, using many theoretical methods, including VCA [36]. A minimal, nearest-neighbor d-wave pairing operator on layer l is defined as

$$\hat{\Delta}^{(l)} = \sum_{\mathbf{r}\in l} c_{\mathbf{r},l,\uparrow}c_{\mathbf{r}+\mathbf{x}^{(l)},l,\downarrow} - c_{\mathbf{r},l,\downarrow}c_{\mathbf{r}+\mathbf{x}^{(l)},l,\uparrow} - c_{\mathbf{r},l,\uparrow}c_{\mathbf{r}+\mathbf{y}^{(l)},l,\downarrow} + c_{\mathbf{r},l,\downarrow}c_{\mathbf{r}+\mathbf{y}^{(l)},l,\uparrow}, \tag{5}$$

where $\mathbf{x}^{(l)}$ and $\mathbf{y}^{(l)}$ are the lattice vectors on layer l. The operators $\hat{\Delta}^{(1,2)}$ have $d_{x^2-y^2}$ symmetry within their own layer in terms of the local axes. However, they do not belong to irreducible representations of the D_4 point group of the bilayer. That point group contains π rotations with respect to axes lying in the plane, exchanging the two layers (see Fig. 2 or Ref. [17]). Under these rotations, the operators $\hat{\Delta}^{(1,2)}$ are interchanged (with phases). We should therefore focus our attention on eigenoperators of the symmetry operations, which fall into the B_1 or B_2 representation of the D_4 point group, defined as

$$\hat{B}_1 = \hat{\Delta}^{(1)} + \hat{\Delta}^{(2)}, \quad \hat{B}_2 = \hat{\Delta}^{(1)} - \hat{\Delta}^{(2)}. \tag{6}$$

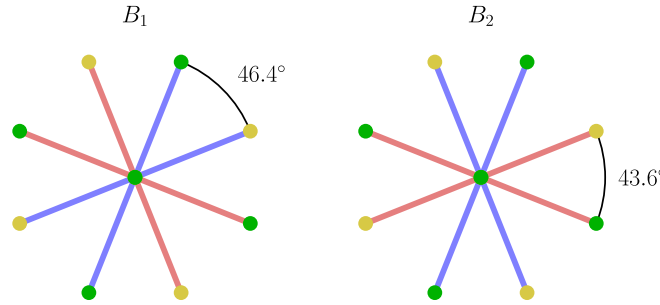

FIG. 2. Schematics of the pairing operators associated with the B_1 and B_2 representations around the pivotal sites (cluster C from Fig. 1). The green (yellow) sites correspond to the top (bottom) layer. Positive (negative) pairing is represented by blue (orange) segments. In the B_1 representation, the links with the same sign are separated by the larger angle (46.4°). In the B_2 representation, they are separated by the smaller angle (43.6°).

These pairing operators are schematically illustrated in Fig. 2. We use the convention from Ref. [17], in which the links with the same sign in the B_1 representation are separated by the large angle (here corresponding to the complementary angle $90° - \theta = 46.4°$). In the B_2 representation, the links with the same sign are separated by the smaller angle (43.6°). At 45°, the two representations are equivalent and should correspond to degenerate states. The same is true if the interlayer hopping V vanishes.

A complex order parameter ψ_a is defined as the average of the pairing operator per site,

$$\psi_a = \frac{1}{L}\langle \hat{B}_a \rangle = \psi'_a + i\psi''_a (a = 1, 2), \tag{7}$$

where ψ'_a and ψ''_a are real and $L = 58$ is the number of sites in the unit cell. Both the B_1 and B_2 states may turn up as valid VCA solutions, but one of them will have a lower energy, depending on doping. If only one of $\psi_{1,2}$ is nonzero, then its phase has no impact and can be set to zero ($\psi''_a = 0$) without loss of generality. However, in the TRS-breaking phase, the two states are close in energy, and the two order parameters may coexist in order to lower the energy further. Since the $B_{1,2}$ states are symmetry eigenstates, the order parameters $\psi_{1,2}$ occur as scalars in the mean-field dispersion relation (the gap function), and the gap is evidently maximized when the two states are in quadrature, i.e., when the two order parameters have a $\pi/2$ phase difference. Since we have the freedom to set $\psi''_1 = 0$, this phase difference implies $\psi'_2 = 0$, and the full gap is then $|\psi'_1 + i\psi''_2| = \sqrt{(\psi'_1)^2 + (\psi''_2)^2}$. However, the phase difference ϕ between $\langle\hat{\Delta}^{(1)}\rangle$ and $\langle\hat{\Delta}^{(2)}\rangle$, i.e., the phase considered in the Josephson description of the bilayer, is different. Since $\hat{\Delta}^{(1,2)} = (\hat{B}_1 \pm \hat{B}_2)/2$,

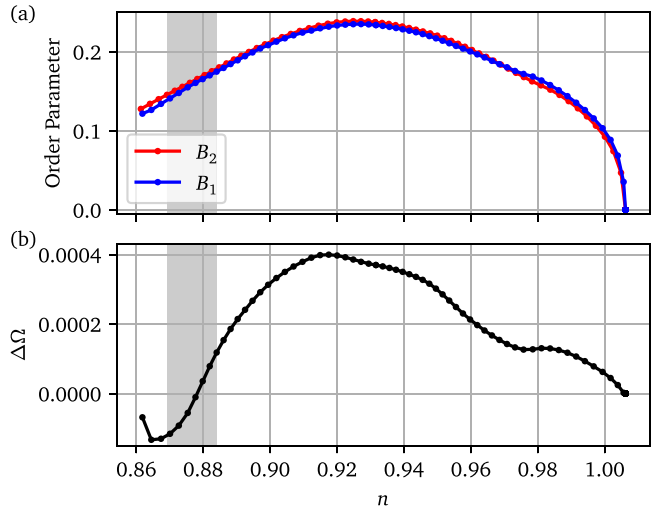

FIG. 3. (a) Norm of the order parameters ψ_1 and ψ_2 obtained from the VCA procedure with a Weiss field belonging, respectively, to the B_1 or B_2 representation for an interlayer hopping of $V = 0.4$ as a function of electron density n. (b) Free energy difference $\Delta\Omega$ between the two states (in units of t). When $\Delta\Omega > 0$ ($\Delta\Omega < 0$) the B_1 (B_2) state is energetically favored. The gray region highlights the density range where TRS breaking is observed (see text).

then

$$\phi = \arg\frac{\psi_1 - \psi_2}{\psi_1 + \psi_2} = \arg\frac{\psi_1' - i\psi_2''}{\psi_1' + i\psi_2''}$$
$$= 2\arg(\psi_1' - i\psi_2'') = -2\arctan\frac{\psi_2''}{\psi_1'}. \quad (8)$$

A value of $\phi = 0$ ($\phi = \pi$) corresponds to a pure B_1 (B_2) case. TRS breaking occurs when $\phi \neq 0$ or π.

To probe the TRS-breaking superconducting phase in the VCA, we simultaneously use as Weiss fields the Hermitian operators $\hat{B}_1 + \hat{B}_1^\dagger$ and $i(\hat{B}_2^\dagger - \hat{B}_2)$ and look for regions of doping where both are nonzero in the VCA solution. This corresponds then to the $B_1 + iB_2$ state. The Weiss fields used in the VCA procedure are taken to be the same on all clusters (except on cluster C, where it is not defined). Using different Weiss fields on different clusters was tested; it did not improve the results significantly and dramatically increased the computational resources needed.

Interlayer pairing operators can also be defined. They were not used as Weiss fields (see Sec. IV of Ref. [17] for an explanation). Nevertheless, interlayer pairing occurs in the sense that the average value of the interlayer pairing operators is nonzero. This pairing propagates from the intralayer pairing through interlayer hopping.

III. RESULT AND DISCUSSION

A. TRS-breaking phase

In this section we consider the parameter describing Bi2212. We start by probing the superconducting phase in model (1) with $\theta = 43.60^\circ$ for types B_1 and B_2 separately. We can compare the energies of the two states and find a doping region where TRS breaking is likely to occur.

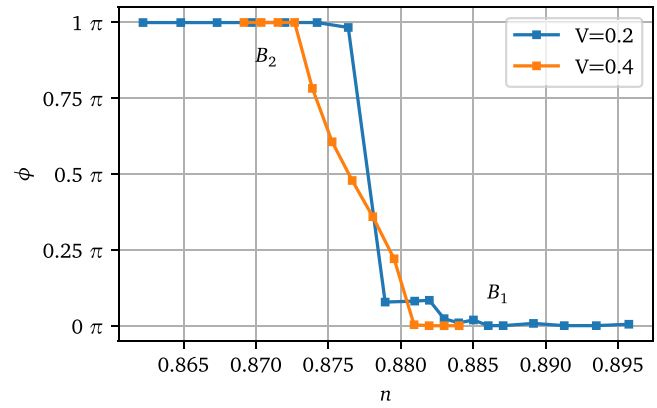

FIG. 4. Relative phase ϕ [Eq. (8)] as a function of n. We can observe a transition from B_1 to B_2 when doping is increased. For $V = 0.4$, a finite region of doping with ϕ between 0 and π is observed, indicating a TRS-breaking phase. For $V = 0.2$, the width of this region, if it exists, is too small to resolve.

In Fig. 3(a), we show the superconducting order parameter for the B_1 and B_2 states for $V = 0.4$. The two states have very similar superconducting domes. The order parameter vanishes around half filling in both cases. That the order parameter does not vanish exactly at $n = 1$ can be attributed to the error on the electron density typical of VCA when the chemical potential within the cluster is not treated as an additional variational parameter.

We can use the optimal value of the Potthoff functional in each state, Ω_{B_1} and Ω_{B_2}, as a measure of the free energy of the system [32]. In Fig. 3(b), we show the difference $\Delta\Omega = \Omega_{B_2} - \Omega_{B_1}$. When $\Delta\Omega$ is positive (negative), the B_1 (B_2) representation is energetically favored.

As shown in Fig. 3(b), the difference $\Delta\Omega$ for $\theta = 43.60^\circ$ is of the order of 10^{-4} (in units of the nearest-neighbor hopping t). For $\theta = 53.13^\circ$, the difference is more of the order of 10^{-3} [17]. This is expected since at 45° the two representations should have the same energy. The closer the twist angle is to 45°, the closer in energy states B_1 and B_2 should be, and TRS breaking should be more likely. For $V = 0.2$, we obtained similar results with an even smaller $\Delta\Omega$, owing to the smaller interlayer tunneling.

We then probed the superconducting phase when the B_1 and B_2 states are simultaneously allowed. The two representations can now compete against each other or combine into a quadrature $B_1 + iB_2$, whichever is energetically favorable. Figure 4 shows the relative phase ϕ computed using Eq. (8) as a function of the density n in a narrow range of density. For $V = 0.2$, it is possible to see an abrupt transition from the B_1 state to the B_2 state. The TRS-breaking region is too narrow to see with our method. The three data points with nonzero ϕ around $n = 0.880$ may be an artifact caused by, e.g., the minimization procedure or the simplified Weiss field configuration used, with the same Weiss field on all clusters.

For $V = 0.4$, the relative phase shows a continuous transition from B_1 to B_2 upon increasing hole doping. We obtain a TRS-breaking state between $n \approx 0.873$ and $n \approx 0.881$. The interlayer tunneling amplitude is the most important parameter controlling the mixing of the two representations, as noted previously [17].

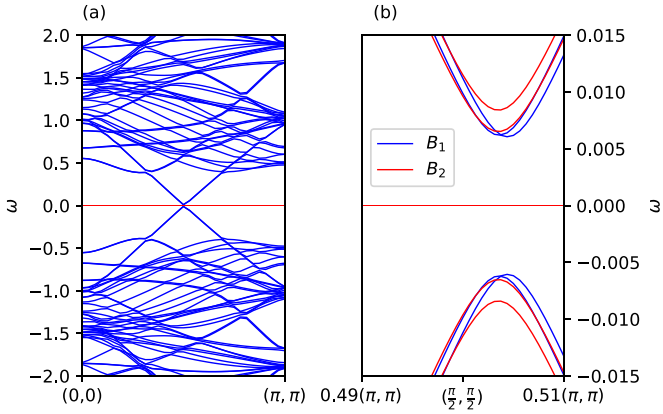

FIG. 5. Band structure of model (1) with $U = 0$ and a superconducting mean field $b_i\hat{B}_i$. (a) Band structure along the diagonal of the first quadrant of the Brillouin zone for $b_1 = 0.2$. The nodes are located around $\mathbf{k} = (\pi/2, \pi/2)$. (b) Close-up of the region around the nodes for $b_1 = 0.2$ (blue) and $b_2 = 0.2$ (red). The nodes are, in fact, slightly gapped for both representations and very close to each other.

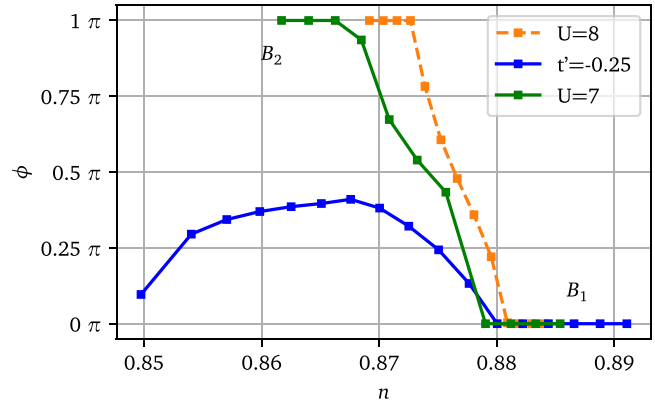

FIG. 6. Relative phase ϕ [Eq. (8)] as a function of n for three parameter sets. In all cases, $t = 1$, and $V = 0.4$. We can observe a finite region of doping with ϕ between 0 and π, indicating a TRS-breaking phase. For $t' = -0.25$, there is no transition between the two possible states: when hole doping is increased, the system starts from a B_1 state, then goes into a TRS-breaking phase, then back to the B_1 state; the doping range is increased when compared to the other data sets. For $U = 0.7$, the behavior is closer to the $U = 8$ case: there is a transition from the B_1 state to B_2 as hole doping is increased. The data for $U = 8$ are the same as those shown in Fig. 4.

The gray area in Fig. 3 highlights the region where TRS breaking is seen in Fig. 4 for $V = 0.4$. It is well beyond optimal doping and corresponds to the range of doping where $\Delta\Omega$ is close to zero.

Our results are similar to those of Ref. [17], where a twist angle of $\theta = 53.13°$ was applied. A TRS-breaking phase near optimal doping was also observed in the strong interlayer regime. The TRS-breaking phase observed with $\theta = 43.60°$ occurs within a smaller doping range, in the overdoped region. It was expected that, closer to 45°, the TRS-breaking phase would occur in a wider doping range. That is not what we observe here.

To explain this, we turn to a simpler approach and consider, at $U = 0$, the effect of a mean field associated with each of the superconducting states, B_1 and B_2, for $\theta = 43.60°$. Usually, we expect an energy gain when combining superconducting states from the same system if the nodes of each state are located at very different positions in the Brillouin zone (BZ). One example of this is the triplet state $p_x + ip_y$. That is not the case in twisted cuprates. One might think that combining a d-wave state from one layer with a d wave from a second layer with a different orientation would effectively do the trick, but in fact, that amounts to combining equivalent representations of two different systems instead of combining two different representations of the same system. In reality, the representations B_1 and B_2 have nodes in the same place.

In Fig. 5(a) we show the band structure of model (1) along the diagonal of the BZ for a nonzero B_1 mean field ($b_1\hat{B}_1$, $b_1 = 0.2$). For a twist angle of $\theta = 43.60°$ there are 58 bands, and the BZ is folded 29 times. There are nodes in the vicinity of $\mathbf{k} = (\pi/2, \pi/2)$ [same for the B_2 state, not shown in Fig. 5(a)]. In Fig. 5(b), we compare the band structures with B_1 and B_2 mean fields around the node (note the enlarged scale). The nodes are not perfect and are, in fact, already gapped for both states: no linear combination $B_1 + iB_2$ is needed to generate the gap. Indeed, when a system has multiple orbitals, the nodes are not necessarily fixed by symmetry [41]. Following this argument, the energy gained by a complex combination $B_1 + iB_2$ can remain small even close to 45°. Hence, the twist angle should not be the only parameter affecting the extent of the TRS-breaking phase or, indeed, the most important one. Other parameters, like doping (discussed in this work) and disorder [42], play a key role.

B. Effect of U and t'

The value of the second-neighbor hopping ($t' = -0.3$) used in the previous section was chosen to describe Bi2212 and to offer a comparison with previous work. We also applied our method to $t' = -0.25$ and $t' = -0.2$, with other parameters staying the same ($t = 1$, $U = 8$, $V = 0.4$). The results for $t' = -0.25$ are shown in Fig. 6 (blue curve). In that case the TRS-breaking phase also appears, but rather as an insertion within the B_1 phase instead of an intermediate state between B_1 and B_2. The doping range over which it appears is also wider (about 3%) but remains small compared to the one observed at $\theta = 53.13°$ in Ref. [17]. At $t' = -0.2$, the B_1 phase always has a lower energy than the B_2 phase, and the TRS-breaking phase does not appear at all. Hence, a larger value of $|t'|$, which entails greater frustration of antiferromagnetic fluctuations, is beneficial to the TRS phase.

We also looked at the effect of the local repulsion U. The green curve in Fig. 6 shows the phase difference ϕ for $t = 1$, $t' = -0.3$, $U = 7$, and $V = 0.4$ (same parameters as in the previous section, but with $U = 7$ instead of $U = 8$). In that case the TRS-breaking phase also occurs but is slightly shifted towards higher doping compared to $U = 8$ (the original parameter set, shown in orange). Additional computations at $U = 10$ also revealed a TRS-breaking solution (not shown here).

Hence, the existence of a TRS-breaking phase is robust with respect to small changes in the model parameters.

However, the precise location of the TRS-breaking phase is affected by the parameters of the single-layer model, more so by the band parameters t' than by the interaction U. In all cases the TRS phase is fragile: the associated energy gain at the twist angle considered here is of the order of $10^{-4}t$, which puts us in the subkelvin range.

IV. CONCLUSION

We used a one-band Hubbard model for twisted bilayer cuprates at $\theta = 43.60^\circ$ with VCA to search for a possible TRS-breaking superconducting phase. In the twisted bilayer, superconductivity is expected away from half filling in either the B_1 or B_2 representation of the D_4 point group. For a set of parameters chosen to describe Bi2212, we found a phase transition from the B_1 state to the B_2 state when doping is increased. A region where the complex combination $B_1 + iB_2$ is stable, thus breaking TRS, occurs in a small range of doping when the interlayer doping is strong enough. Our results are in accord with previous work on the 53.13° system, in which the observation of TRS breaking needed a strong interlayer tunneling [17]. We also showed that the two states B_1 and B_2 are closer in energy when the twist angle approaches 45°, where they are expected to be equivalent.

The energy difference between the two states being smaller as the twist angle approaches 45° makes it harder to probe TRS breaking. With a simple mean-field argument, we showed that the nodes of the B_1 and B_2 states are very close, making the energy gain from combining them very small. Hence, the twist angle cannot be the only parameter controlling the TRS breaking. The doping level needs to be considered, alongside the twist angle and probably disorder level, to create a robust TRS-breaking state.

We also looked at the effect of the model parameters. We found that the TRS-breaking phase is robust against small variations of t' and U but that it is negatively impacted by smaller values of $|t'|$, i.e., by smaller AF frustration. At the same time, the TRS phase occurs on only the overdoped side of the dome, i.e., in the more weakly correlated region of the phase diagram. These two observations go in the same direction; that is, strongly correlated superconductivity mediated by antiferromagnetic fluctuations is more hindrance than help to the TRS-breaking phase. The TRS phase also requires a large interlayer hopping amplitude, larger than what can be expected in real materials, to be present in a significant doping range.

The system studied here is made of two layers of the same cuprate model, with the same doping. Taking inspiration from the heterobilayer transition metal dichalcogenides [5,11], layers of different cuprates might be used to stabilize the TRS-breaking state. The difference in doping and structure might lead to a change in the TRS-breaking region. We will address this question in a future work.

ACKNOWLEDGMENTS

This work was supported by the Natural Sciences and Engineering Research Council of Canada (NSERC) under Grant No. RGPIN-2020-05060, by the NSERC postgraduate scholarships doctoral program, and by Fonds de Recherche du Québec Nature et technologies (FRQNT) doctoral research scholarships. Computational resources were provided by the Digital Research Alliance of Canada and Calcul Québec.

[1] Y. Cao, V. Fatemi, A. Demir, S. Fang, S. L. Tomarken, J. Y. Luo, J. D. Sanchez-Yamagishi, K. Watanabe, T. Taniguchi, E. Kaxiras, R. C. Ashoori, and P. Jarillo-Herrero, Nature (London) **556**, 80 (2018).

[2] Y. Cao, V. Fatemi, S. Fang, K. Watanabe, T. Taniguchi, E. Kaxiras, and P. Jarillo-Herrero, Nature (London) **556**, 43 (2018).

[3] L. Balents, C. R. Dean, D. K. Efetov, and A. F. Young, Nat. Phys. **16**, 725 (2020).

[4] L. Xian, D. M. Kennes, N. Tancogne-Dejean, M. Altarelli, and A. Rubio, Nano Lett. **19**, 4934 (2019).

[5] D. A. Ruiz-Tijerina and V. I. Fal'ko, Phys. Rev. B **99**, 125424 (2019).

[6] L. Wang, E.-M. Shih, A. Ghiotto, L. Xian, D. A. Rhodes, C. Tan, M. Claassen, D. M. Kennes, Y. Bai, B. Kim, K. Watanabe, T. Taniguchi, X. Zhu, J. Hone, A. Rubio, A. N. Pasupathy, and C. R. Dean, Nat. Mater. **19**, 861 (2020).

[7] L. An, X. Cai, D. Pei, M. Huang, Z. Wu, Z. Zhou, J. Lin, Z. Ying, Z. Ye, X. Feng, R. Gao, C. Cacho, M. Watson, Y. Chen, and N. Wang, Nanoscale Horiz. **5**, 1309 (2020).

[8] Z. Zhang, Y. Wang, K. Watanabe, T. Taniguchi, K. Ueno, E. Tutuc, and B. J. LeRoy, Nat. Phys. **16**, 1093 (2020).

[9] S. Venkateswarlu, A. Honecker, and G. Trambly de Laissardiére, Phys. Rev. B **102**, 081103(R) (2020).

[10] E. C. Regan, D. Wang, C. Jin, M. I. Bakti Utama, B. Gao, X. Wei, S. Zhao, W. Zhao, Z. Zhang, K. Yumigeta, M. Blei, J. D. Carlström, K. Watanabe, T. Taniguchi, S. Tongay, M. Crommie, A. Zettl, and F. Wang, Nature (London) **579**, 359 (2020).

[11] Y. Tang, L. Li, T. Li, Y. Xu, S. Liu, K. Barmak, K. Watanabe, T. Taniguchi, A. H. MacDonald, J. Shan, and K. F. Mak, Nature (London) **579**, 353 (2020).

[12] M. Bélanger, J. Fournier, and D. Sénéchal, Phys. Rev. B **106**, 235135 (2022).

[13] Y. Yu, L. Ma, P. Cai, R. Zhong, C. Ye, J. Shen, G. D. Gu, X. H. Chen, and Y. Zhang, Nature (London) **575**, 156 (2019).

[14] S. Y. F. Zhao, N. Poccia, M. G. Panetta, C. Yu, J. W. Johnson, H. Yoo, R. Zhong, G. D. Gu, K. Watanabe, T. Taniguchi, S. V. Postolova, V. M. Vinokur, and P. Kim, Phys. Rev. Lett. **122**, 247001 (2019).

[15] O. Can, T. Tummuru, R. P. Day, I. Elfimov, A. Damascelli, and M. Franz, Nat. Phys. **17**, 519 (2021).

[16] P. A. Volkov, J. H. Wilson, K. P. Lucht, and J. H. Pixley, Phys. Rev. B **107**, 174506 (2023).

[17] X. Lu and D. Sénéchal, Phys. Rev. B **105**, 245127 (2022).

[18] G. Margalit, B. Yan, M. Franz, and Y. Oreg, Phys. Rev. B **106**, 205424 (2022).

[19] A. Mercado, S. Sahoo, and M. Franz, Phys. Rev. Lett. **128**, 137002 (2022).

[20] T. Tummuru, É. Lantagne-Hurtubise, and M. Franz, Phys. Rev. B **106**, 014520 (2022).
[21] M. Martini, Y. Lee, T. Confalone, S. Shokri, C. N. Saggau, D. Wolf, G. Gu, K. Watanabe, T. Taniguchi, D. Montemurro, V. M. Vinokur, K. Nielsch, and N. Poccia, Materials Today **67**, 106 (2023).
[22] Y. Lee, M. Martini, T. Confalone, S. Shokri, C. N. Saggau, D. Wolf, G. Gu, K. Watanabe, T. Taniguchi, D. Montemurro, V. M. Vinokur, K. Nielsch, and N. Poccia, Adv. Mater. **35**, 2209135 (2023).
[23] Y. Zhu, M. Liao, Q. Zhang, H.-Y. Xie, F. Meng, Y. Liu, Z. Bai, S. Ji, J. Zhang, K. Jiang, R. Zhong, J. Schneeloch, G. Gu, L. Gu, X. Ma, D. Zhang, and Q.-K. Xue, Phys. Rev. X **11**, 031011 (2021).
[24] J. Lee, W. Lee, G.-Y. Kim, Y.-B. Choi, J. Park, S. Jang, G. Gu, S.-Y. Choi, G. Y. Cho, G.-H. Lee, and H.-J. Lee, Nano Lett. **21**, 10469 (2021).
[25] S. Y. F. Zhao, X. Cui, P. A. Volkov, H. Yoo, S. Lee, J. A. Gardener, A. J. Akey, R. Engelke, Y. Ronen, R. Zhong, G. Gu, S. Plugge, T. Tummuru, M. Kim, M. Franz, J. H. Pixley, N. Poccia, and P. Kim, Science **382**, 1422 (2023).
[26] P. A. Volkov, S. Y. F. Zhao, N. Poccia, X. Cui, P. Kim, and J. H. Pixley, arXiv:2108.13456.
[27] T. Tummuru, S. Plugge, and M. Franz, Phys. Rev. B **105**, 064501 (2022).
[28] S. S. Dash and D. Sénéchal, Phys. Rev. B **100**, 214509 (2019).
[29] X.-Y. Song, Y.-H. Zhang, and A. Vishwanath, Phys. Rev. B **105**, L201102 (2022).
[30] D. Sénéchal, A. G. R. Day, V. Bouliane, and A.-M. S. Tremblay, Phys. Rev. B **87**, 075123 (2013).
[31] R. S. Markiewicz, S. Sahrakorpi, M. Lindroos, H. Lin, and A. Bansil, Phys. Rev. B **72**, 054519 (2005).
[32] M. Potthoff, M. Aichhorn, and C. Dahnken, Phys. Rev. Lett. **91**, 206402 (2003).
[33] C. Dahnken, M. Aichhorn, W. Hanke, E. Arrigoni, and M. Potthoff, Phys. Rev. B **70**, 245110 (2004).
[34] P. Sahebsara and D. Sénéchal, Phys. Rev. Lett. **100**, 136402 (2008).
[35] M. Laubach, J. Reuther, R. Thomale, and S. Rachel, Phys. Rev. B **90**, 165136 (2014).
[36] D. Sénéchal, P. L. Lavertu, M.-A. Marois, and A.-M. S. Tremblay, Phys. Rev. Lett. **94**, 156404 (2005).
[37] J. P. L. Faye and D. Sénéchal, Phys. Rev. B **95**, 115127 (2017).
[38] M. Potthoff, in *Strongly Correlated Systems: Theoretical Methods*, edited by A. Avella and F. Mancini, Springer Series in Solid-State Sciences, Vol. 176 (Springer, Berlin, 2012), pp. 303–339.
[39] M. Potthoff, in *DMFT at 25 Infinite Dimensions*, edited by E. Pavarini, E. Koch, A. Lichtenstein, and D. Vollhardt, Schriften des Forschungszentrums Jülich Series Modelling and Simulation Vol. 4 (Forschungszentrum Jülich, Jülich, Germany, 2014), pp. 9.1–9.36.
[40] T. A. Maier, M. Jarrell, T. C. Schulthess, P. R. C. Kent, and J. B. White, Phys. Rev. Lett. **95**, 237001 (2005).
[41] S.-O. Kaba and D. Sénéchal, Phys. Rev. B **100**, 214507 (2019).
[42] A. C. Yuan, Y. Vituri, E. Berg, B. Spivak, and S. A. Kivelson, Phys. Rev. B **108**, L100505 (2023).